IMMUNOLOGY

Inhibition of neutrophil extracellular trap formation alleviates vascular dysfunction in type 1 diabetic mice

Chao Liu[1], Srilakshmi Yalavarthi[1], Ajay Tambralli[1], Lixia Zeng[2], Christine E. Rysenga[1], Nikoo Alizadeh[1], Lucas Hudgins[1], Wenying Liang[1], Somanathapura K. NaveenKumar[1], Hui Shi[1,3], Miriam A. Shelef[4,5], Kevin B. Atkins[2], Subramaniam Pennathur[2,6], Jason S. Knight[1]*

While neutrophil extracellular traps (NETs) have previously been linked to some diabetes-associated complications, such as dysfunctional wound healing, their potential role in diabetic vascular dysfunction has not been studied. Diabetic Akita mice were crossed with either *Elane*$^{-/-}$ or *Pad4*$^{-/-}$ mice to generate NET-deficient diabetic mice. By 24 weeks of age, Akita aortae showed markedly impaired relaxation in response to acetylcholine, indicative of vascular dysfunction. Both Akita-*Elane*$^{-/-}$ mice and Akita-*Pad4*$^{-/-}$ mice had reduced levels of circulating NETs and improved acetylcholine-mediated aortic relaxation. Compared with wild-type aortae, the thromboxane metabolite TXB_2 was roughly 10-fold higher in both intact and endothelium-denuded aortae of Akita mice. In contrast, Akita-*Elane*$^{-/-}$ and Akita-*Pad4*$^{-/-}$ aortae had TXB_2 levels similar to wild type. In summary, inhibition of NETosis by two independent strategies prevented the development of vascular dysfunction in diabetic Akita mice. Thromboxane was up-regulated in the vessel walls of NETosis-competent diabetic mice, suggesting a role for neutrophils in driving the production of this vasoconstrictive and atherogenic prostanoid.

INTRODUCTION

Diabetes mellitus is a prevalent disease characterized by hyperglycemia. Diabetes is associated with an increased risk of cardiovascular complications such as myocardial infarction and stroke, which are major causes of mortality in individuals with both type 1 and type 2 diabetes (*1*, *2*). Preclinical vascular dysfunction in diabetic patients predicts the development of atherosclerosis and is correlated with negative outcomes (*3*, *4*).

A recent study found that levels of circulating neutrophils were positively correlated with the risk of cardiovascular complications in diabetic patients (*5*). Furthermore, exaggerated neutrophil extracellular trap (NET) formation, also known as NETosis, has been observed in individuals with both type 1 and type 2 diabetes (*6*, *7*). NETosis is a unique form of cell death that differs from necrosis and apoptosis (*8*, *9*). As part of the innate immune response against various microorganisms, NETs are extracellular webs of decondensed chromatin and granular contents that together help neutralize entrapped pathogens. NETosis can also be triggered by sterile stimuli (*9*, *10*) such as cytokines, cholesterol crystals, immune complexes, and autoantibodies (*11*). In diabetes, the degree of NETosis correlates with and appears to be at least partially driven by hyperglycemia (*6*), which has been confirmed in various rodent models (*12*, *13*). Meanwhile, in type 2 diabetes, inflammatory cytokines (tumor necrosis factor–α and interleukin-6) and homocysteine may further amplify NETosis (*14*, *15*). While blocking NETosis has been shown to improve wound healing in diabetic mice (*13*, *16*, *17*), the relationship between diabetes, NETosis, and early vascular dysfunction remains to be characterized.

In most contexts, NETosis requires the stepwise generation of reactive oxygen species (ROS) by either the nicotinamide adenine dinucleotide phosphate (NADPH) oxidase complex or mitochondria, the migration of granular components such as neutrophil elastase and myeloperoxidase (MPO) to the nucleus where they initiate the decondensation of chromatin, and the deimination of histones by peptidylarginine deiminase type 4 (PAD4) leading to full chromatin decondensation (*18*). Numerous groups have leveraged pharmacological inhibition of neutrophil elastase as a strategy for preventing NETosis in vivo, particularly in cancer studies (*19*, *20*). Another approach to abolishing the function of neutrophil elastase is through its gene knockout (*Elane*$^{-/-}$), such as in models of experimental atherosclerosis (*21*). The pan-PAD inhibitor Cl-amidine has also been used to inhibit NETosis in vivo (*22*–*25*), while *Pad4*$^{-/-}$ mice also demonstrate NETosis deficiency (*26*–*28*).

The endothelium regulates vascular smooth muscle tone through the production of nitric oxide (*29*), with a loss of nitric oxide production being a hallmark of the preclinical vascular dysfunction that precedes histologically apparent vascular disease such as atherosclerosis. Meanwhile, the vessel wall is also a source of vasoactive prostanoids such as prostacyclin (a vasodilator) and thromboxane (TXA_2, typically a vasoconstrictor) that are derived from arachidonic acid. While platelets are the best-known source of TXA_2, various other cells, including neutrophils (*30*–*32*), may also be a source.

NETosis has been revealed to play an important role in the vascular dysfunction characteristic of many diseases. For example, NETs contribute to the development of hypertension by promoting vascular smooth muscle cell (VSMC) phenotypic shifts (*33*) and impair normal vascular remodeling during stroke recovery (*34*). NETs also appear to propel arterial/venous thrombosis in cancer

[1]Division of Rheumatology, Department of Internal Medicine, University of Michigan, Ann Arbor, MI, USA. [2]Division of Nephrology, Department of Internal Medicine, University of Michigan, Ann Arbor, MI, USA. [3]Department of Rheumatology and Immunology, Ruijin Hospital, School of Medicine, Shanghai Jiao Tong University, Shanghai, China. [4]Division of Rheumatology, Department of Medicine, University of Wisconsin–Madison, Madison, WI, USA. [5]William S. Middleton Memorial Veterans Hospital, Madison, WI, USA. [6]Department of Molecular and Integrative Physiology, University of Michigan, Ann Arbor, MI, USA.
*Corresponding author. Email: jsknight@umich.edu

(*35*), systemic lupus erythematosus (*36*), antiphospholipid syndrome (*37*), and COVID-19 (*38*).

Here, we hypothesized that NETs might be important disruptors of vascular function in diabetic vessels. We explored the NETosis activity and bioenergetic profiles of the neutrophils of diabetic mice. Macrovascular (aorta) endothelial and smooth muscle function were tested by wire myography, including in mice in which NETosis had been blocked either genetically or pharmacologically. We also transferred diabetic neutrophils into young, healthy mice to assess their impact on vascular function. Last, we measured different prostanoid metabolites in the vessel wall and studied the relationship between NETosis, TXA_2, and vascular dysfunction.

RESULTS

Evidence of vascular dysfunction and neutrophil hyperactivity in Akita mice

Because of a mutation in the proinsulin gene, Akita mice, as a model of type 1 diabetes, develop hypoinsulinemia and hyperglycemia by 4 weeks of age, with blood glucose levels consistently >750 mg/dl by the 24-week time point used for most of the following experiments. Akita mice do not develop obesity. While increased NETosis has been observed in other mouse models of type 1 diabetes (*13*, *39*, *40*), this question has not, to our knowledge, been previously addressed in Akita mice. Here, we found that, as compared with wild-type (WT) mice, 24-week-old Akita mice demonstrated more NET remnants in circulation as measured by MPO-DNA complexes (Fig. 1A). Neutrophils from Akita mice did not though differ in their expression of the genes that code for the glucose transporters GLUT1, GLUT2, GLUT3, or GLUT4 (fig. S1). To confirm that 24-week-old Akita mice also develop vascular dysfunction, aortic rings were characterized ex vivo by wire myography. After a standard precontraction of the rings with phenylephrine (PE), relaxation in response to stepwise increasing concentrations of acetylcholine was significantly diminished in Akita mice, indicating endothelial dysfunction (Fig. 1B). The difference between WT and Akita mice was also apparent when plotted as E_{max} values (maximum relaxation calculated by nonlinear regression; Fig. 1C). Aortic smooth muscle function was also tested in 24-week-old Akita and WT mice. Akita mice showed a slightly blunted response to increasing concentrations of sodium nitroprusside (Fig. 1D), which was statistically significant when analyzed as E_{max} (Fig. 1E).

We next characterized the bioenergetic profiles of thioglycolate-elicited peritoneal neutrophils isolated from 24-week-old Akita mice. The Akita neutrophils demonstrated increased glycolytic reserve (Fig. 2, A and B), the difference between baseline glycolysis (fig. S2A) and glycolytic capacity (fig. S2B). Suggestive of mitochondrial dysfunction, Akita neutrophils also demonstrated reduced spare respiratory capacity (Fig. 2, C and D), the difference between basal (fig. S2C) and maximal (fig. S2D) respiration.

We also measured the oxygen consumption rate (OCR) upon exposure of neutrophils to the NADPH oxidase activator phorbol 12-myristate 13-acetate (PMA). As compared with WT neutrophils, the Akita neutrophils demonstrated a more robust oxidative burst (Fig. 2E), which could be quantified by plotting maximum OCR relative to baseline (Fig. 2F). Last, we asked whether the increased oxidative burst would lead to more NETosis. The Akita neutrophils demonstrated more NETosis in response to PMA (Fig. 2, G and H). In summary, these data indicate that aged Akita mice demonstrate endothelial and, to a lesser extent, smooth muscle dysfunction. Neutrophils from the Akita mice also appear to be bioenergetically primed for enhanced NETosis.

Knockout of *Elane* or *Pad4* prevents vascular dysfunction in Akita mice

In an independent cohort of mice from those described in Fig. 1, we measured blood glucose in 24-week-old Akita mice and found no significant differences in the presence of either *Elane* or *Pad4* deficiency (Fig. 3A). In contrast, levels of circulating NET remnants were significantly diminished by both gene knockouts (Fig. 3B). We then assessed endothelial and smooth muscle function of aortic rings by ex vivo wire myography. As compared with Akita mice, both Akita-*Elane*$^{-/-}$ and Akita-*Pad4*$^{-/-}$ mice demonstrated significantly improved endothelial function, as defined by acetylcholine-mediated relaxation of aortic rings (Fig. 3, C and D). In further support of restoration of endothelial homeostasis, we also found evidence of increased circulating intercellular adhesion molecule–1 (ICAM-1) in Akita mice, which was rescued by the *Elane* and *Pad4* mutations (fig. S3). Although the magnitude of the change was more subtle, *Pad4* knockout also improved the smooth muscle function of Akita mice (fig. S4). In summary, these data demonstrate that two different gene mutations that reduce NETosis also improve the vascular function of Akita mice.

Administration of a neutrophil elastase inhibitor to aged Akita mice reverses vascular dysfunction

We next asked whether neutrophil inhibition might reverse vascular dysfunction that had already developed in Akita mice. Beginning at 24 weeks of age, Akita mice began receiving chow supplemented with either the neutrophil elastase inhibitor GW311616A or vehicle control (Fig. 4A). While blood glucose levels were not affected by the inhibitor (Fig. 4B), the vascular function of Akita mice in response to acetylcholine was significantly improved (Fig. 4, C and D). In summary, these data suggest that there is potential for NETosis inhibition to not only prevent vascular dysfunction but also reverse it once it has developed.

Induction of vascular dysfunction upon transfer of Akita neutrophils into WT mice

To further assess the extent to which the Akita vascular phenotype was at least partially attributable to neutrophils, we transferred neutrophils from aged Akita mice into young WT mice (Fig. 5A). Such neutrophils were typically of high purity and did not include detectable platelet or platelet-derived microvesicle contamination (fig. S5). Twenty-four hours after transfer, we found evidence of vascular dysfunction in response to acetylcholine upon transfer of Akita, but not Akita-*Elane*$^{-/-}$ or Akita-*Pad4*$^{-/-}$ neutrophils into WT mice (Fig. 5, B and C). We further confirmed that the bone marrow–derived Akita neutrophils used in these experiments demonstrated a reduced threshold for NETosis as compared with WT, Akita-*Elane*$^{-/-}$, or Akita-*Pad4*$^{-/-}$ neutrophils (Fig. 5, D and E). Together, these data indicate that Akita neutrophils have the potential to trigger vascular dysfunction.

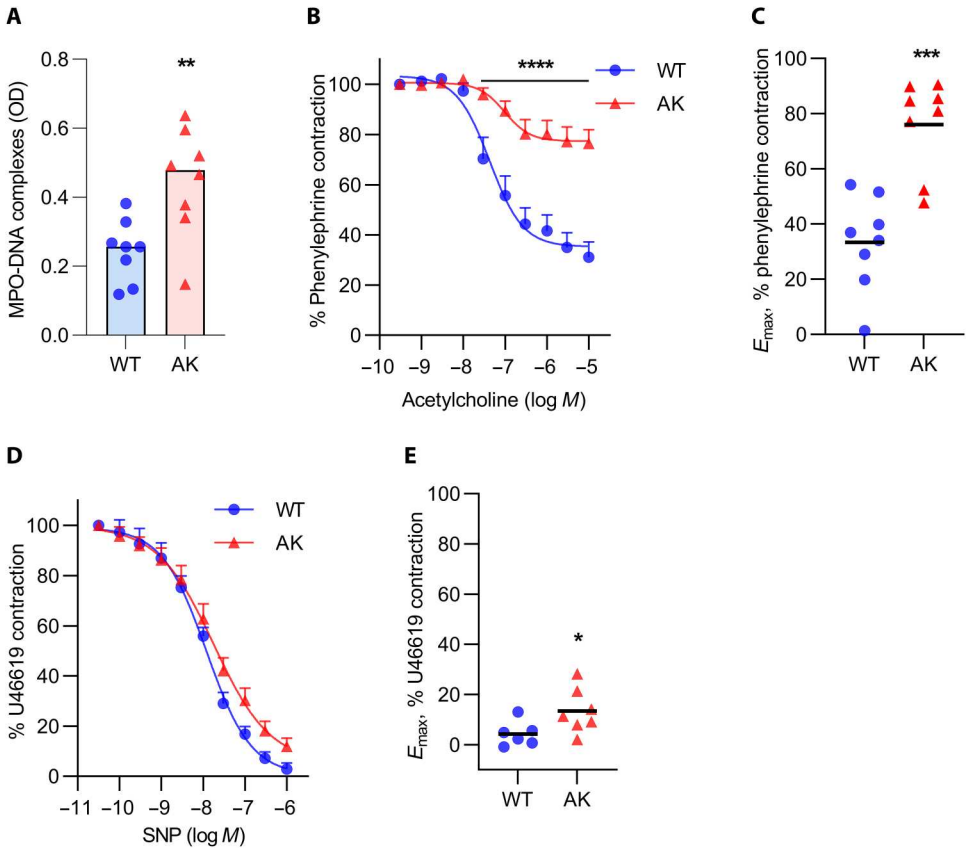

Fig. 1. Vascular dysfunction in 24-week-old Akita mice. (**A**) Optical density (OD) of plasma myeloperoxidase (MPO)–DNA complexes; mean for $n = 8$, $^{**}P < 0.01$ by unpaired Student's t test. (**B**) Relaxation of aortic rings in response to acetylcholine (Ach) after achieving a stable phenylephrine (PE) contraction plateau. Data are presented relative to the force remaining from the PE contraction, which was set as 100%; means + SEM for $n = 8$, $^{****}P < 0.0001$ compared with WT mice by two-way analysis of variance (ANOVA) followed by the Holm-Šídák test. (**C**) Maximal efficacy (E_{max}) values as determined by nonlinear regression analysis; mean for $n = 8$, $^{***}P < 0.001$ compared with the WT mice by unpaired Student's t test. (**D**) Relaxation of aortic rings in response to sodium nitroprusside (SNP) after achieving a stable U46619 contraction plateau. Data are presented relative to the force remaining from the U46619 contraction, which was set as 100%; means + SEM for $n = 6$ to 7. (**E**) E_{max} values as determined by nonlinear regression analysis; mean for $n = 6$ to 7, $^{*}P < 0.05$ compared with WT mice by unpaired Student's t test. AK, Akita.

Increased thromboxane in Akita aortae contributes to vascular dysfunction

Because prostanoids play an indispensable and potentially modifiable role in vascular function, we profiled various prostanoid metabolites by liquid chromatography–mass spectrometry in intact or endothelium-denuded aortae. We found that the thromboxane metabolite TXB_2 (a more stable surrogate for TXA_2) was present at increased levels in the aortae of Akita mice as compared with WT mice, whether the endothelium was intact or removed (Fig. 6, A and B, and fig. S6A). Similar differences were also appreciated when comparing the Akita aortae to those of either Akita-*Elane*$^{-/-}$ or Akita-*Pad4*$^{-/-}$ mice (Fig. 6, A and B). We also detected a potentially compensatory up-regulation of 15-deoxy-PGJ_2 [a dehydration product of PGD_2 and potent peroxisome proliferator–activated receptor–γ (PPAR-γ) agonist] in the intact aortae of Akita mice (Fig. 6C) that was lost with removal of the endothelium (Fig. 6D and fig. S6B). No differences were appreciated for any of the other detected prostanoids (fig. S7, A to H).

After discovering the up-regulation of TXB_2 in Akita mice aortae, we tested the impact of furegrelate, a thromboxane synthase inhibitor, on Akita vascular function in response to acetylcholine. The addition of furegrelate to the aortic rings restored Akita vascular function to that seen in WT mice (Fig. 6, E and F). We also measured the expression of various prostanoid-regulating enzymes, including thromboxane synthase, in Akita neutrophils. As compared with WT, the expression of the gene encoding thromboxane synthase was significantly up-regulated in Akita neutrophils (Fig. 6G). This was accompanied by more TXB_2 in the supernatants of stimulated Akita neutrophils (Fig. 6H). Together, these data suggest that vessel-wall thromboxane, potentially of neutrophil origin, contributes to the preclinical vascular dysfunction of diabetic Akita mice.

DISCUSSION

Our study confirmed preclinical vascular dysfunction in Akita mice, as has been reported previously (*29*). To address the potential relationship between diabetes, NETosis, and this macrovascular dysfunction, we used two gene-knockout mouse strains: neutrophil elastase-knockout (*Elane*$^{-/-}$) and PAD4-knockout (*Pad4*$^{-/-}$) mice. As compared with gene-sufficient Akita mice, the Akita knockout mice demonstrated not only reduced NET remnants in

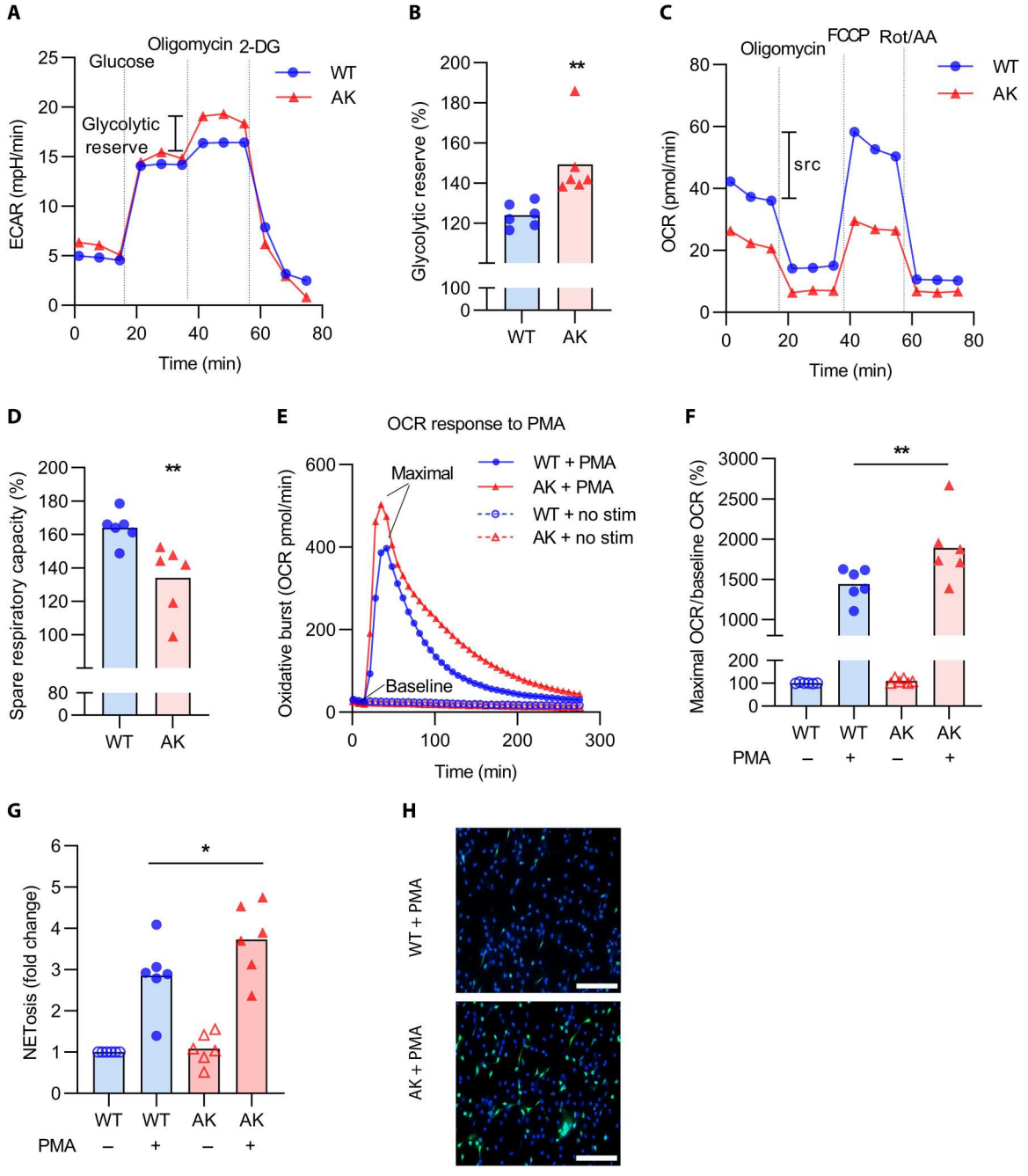

Fig. 2. Phenotypic characterization of neutrophils in 24-week-old Akita mice. (**A**) Representative extracellular acidification rate (ECAR) curves assessing glycolysis. (**B**) Glycolytic reserve is the difference between glycolytic capacity and baseline glycolysis; mean for $n = 6$, $^{**}P < 0.01$ compared with WT mice by unpaired Student's t test. (**C**) Representative oxygen consumption rate (OCR) curves assessing mitochondrial respiration. (**D**) The spare respiratory capacity (src) is the difference between maximal and basal respiration; mean for $n = 6$, $^{**}P < 0.01$ compared with WT mice by unpaired Student's t test. (**E**) Representative OCR curves indicative of the oxidative burst after PMA stimulation. (**F**) Maximal OCR relative to baseline OCR; mean for $n = 6$, $^{**}P < 0.01$ by one-way ANOVA followed by the Holm-Šídák test. (**G**) NETosis after PMA stimulation measured by SYTOX staining; mean for $n = 6$ to 7, $^{*}P < 0.05$ by one-way ANOVA followed by the Holm-Šídák test. (**H**) Representative microscopy indicating NETosis; blue, DNA; green, neutrophil elastase. Scale bars, 100 μm.

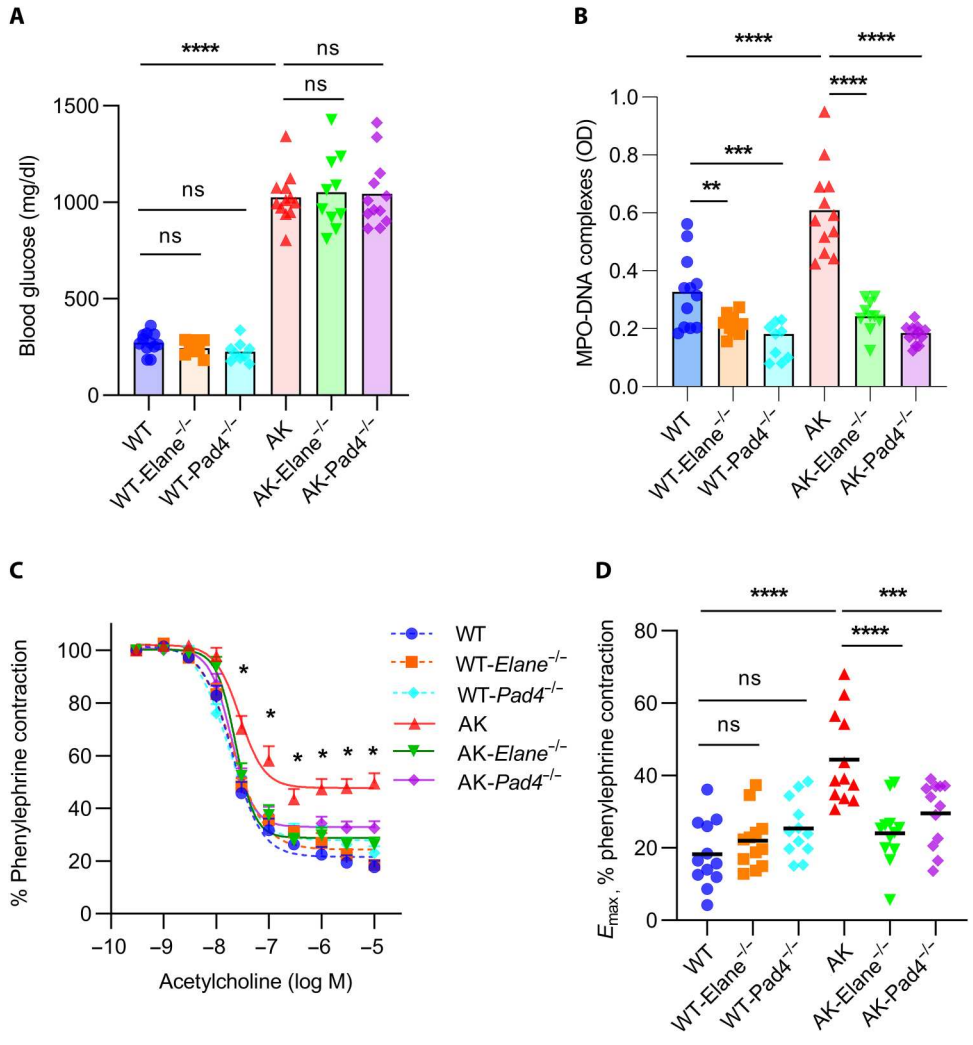

Fig. 3. Improved vascular function in Akita-*Elane*$^{-/-}$ and Akita-*Pad4*$^{-/-}$ aortae as compared with Akita aortae. (**A**) Glucose levels were tested in the plasma of all groups; mean for $n = 9$ to 12, $^{****}P < 0.0001$, Akita mice compared with WT mice by one-way ANOVA followed by the Holm-Šídák test, ns, not significant. (**B**) OD values of MPO-DNA complex ELISA; mean for $n = 9$ to 12, $^{**}P < 0.01$, $^{***}P < 0.001$, and $^{****}P < 0.0001$ by one-way ANOVA followed by the Holm-Šídák test. (**C**) Relaxation of aortic rings in response to acetylcholine (Ach) after achieving a stable phenylephrine (PE) contraction plateau. Data are presented relative to the force remaining from the PE contraction, which was set as 100%; mean + SEM for $n = 12$, $^{*}P < 0.05$, Akita mice compared with each other group by two-way ANOVA followed by the Holm-Šídák test. (**D**) E_{max} values as determined by nonlinear regression analysis; mean for $n = 12$, $^{***}P < 0.001$ and $^{****}P < 0.0001$ by one-way ANOVA followed by the Holm-Šídák test.

circulation but also improved vascular function. Furthermore, experiments with a neutrophil elastase inhibitor showed the potential for reversal of diabetic vascular dysfunction that had already developed, while cell transfer experiments implicated neutrophils as at least one driver of the dysfunction. Our data also raise the possibility that production of thromboxane in the vessel wall and/or perivascular tissue related to neutrophils is a driver of diabetic vascular dysfunction.

Akita neutrophils showed not only higher NETosis activity but also an enhanced potential to engage glycolysis and produce a more robust oxidative burst when stimulated with PMA. Neutrophils mainly rely on glycolysis for energy production and have relatively fewer mitochondria than other immune cells (*41*). This reliance on glycolysis also appears to be true during NETosis (*41*), as indicated by reports that NETosis induced by PMA and amyloid fibrils is inhibited by 2-deoxyglucose, which blocks hexokinase function (*42*, *43*). PMA- and amyloid fibril–induced NET formation can also be inhibited by suppressing the pentose phosphate pathway, which supports ROS production in neutrophils through the generation of NADPH to be used by the NADPH oxidase complex (*43*). Together, Akita neutrophils showed lower OCR (spare respiratory capacity) in the context of standard inhibitors for characterizing mitochondrial function but showed higher OCR after PMA stimulation, for which one possible explanation is that Akita neutrophils are able to engage glycolysis to increase flux through the pentose phosphate pathway, generating NADPH that is then readily available for the oxidative burst that consumes oxygen.

Numerous strategies have been suggested for inhibiting NETosis. Examples include neutralization of NETosis-promoting ligands and/or their receptors (*44*), preventing efficient chromatin decondensation (*26*, *45*, *46*), suppressing energy utilization and/or the oxidative burst (*47*), and directing neutrophils away from

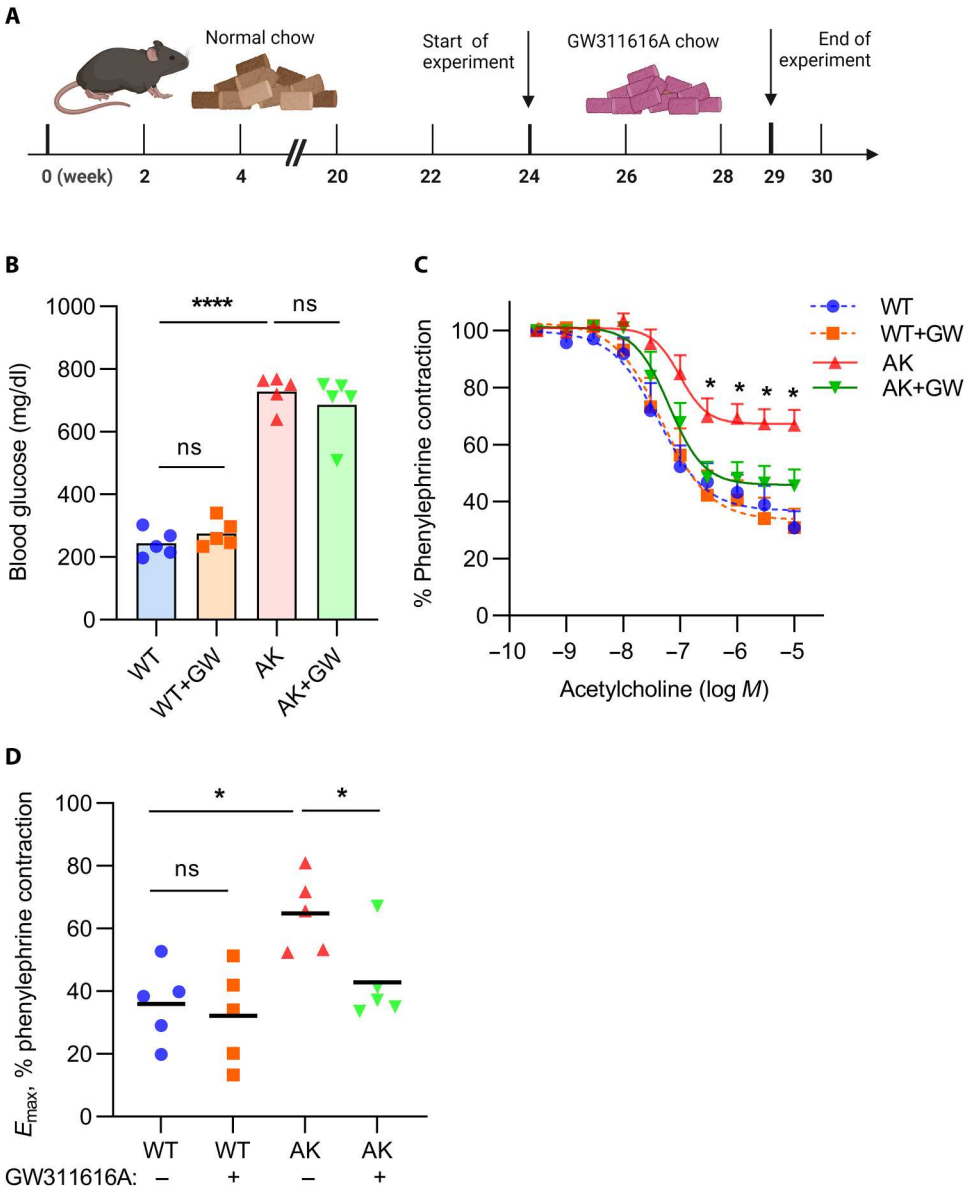

Fig. 4. Improved vascular function when aged Akita mice are treated with a neutrophil elastase inhibitor. (**A**) Twenty-four–week–old mice were treated with chow containing GW311616A for 5 weeks; schematic prepared with biorender.com. (**B**) Glucose levels were tested in the plasma of all groups; mean for $n = 5$, ****$P < 0.0001$ Akita mice compared with WT mice by one-way ANOVA followed by the Holm-Šídák test. (**C**) Relaxation of aortic rings in response to acetylcholine (Ach) after achieving a stable phenylephrine (PE) contraction plateau. Data are presented relative to the force remaining from the PE contraction, which was set as 100%; means + SEM for $n = 5$ to 6, *$P < 0.05$ Akita mice compared with each other group by two-way ANOVA followed by the Holm-Šídák test. (**D**) E_{max} values as determined by nonlinear regression analysis; mean for $n = 5$ to 6, *$P < 0.05$ by one-way ANOVA followed by the Holm-Šídák test.

NETosis and toward apoptosis (*48*, *49*). The approaches used here likely focus primarily on chromatin decondensation. Beyond the *Elane*$^{-/-}$ (*21*) and *Pad4*$^{-/-}$ (*26*–*28*) mice, we used GW311616A as a pharmacological approach to inhibit NETosis. This agent has previously been reported to have good oral bioavailability along with strong and specific neutrophil elastase-inhibiting effects (*50*). We found that GW311616A reduced vascular dysfunction in 24-week-old Akita mice after 5 weeks of treatment, which aligns well with previous work assessing the impact of this drug on frank atherosclerosis in mice (*21*). While no neutrophil elastase inhibitors are currently approved for use in the United States, sivelestat was approved in Japan as a drug for acute lung injury associated with systemic inflammatory response syndrome (*51*). Future studies may move beyond the lungs to assess the impact of neutrophil elastase inhibition on vascular disease in humans.

We acknowledge that inhibition of neutrophil elastase and PAD4 may have effects that extend beyond neutrophils. For example, PAD4 can citrullinate both histones and nonhistone proteins, regulating gene transcription alone or in combination with other post-translational modifications in various biological processes (*52*). Neutrophil elastase is a major protease of neutrophil granules. Beyond its role in combatting infections, neutrophil elastase has

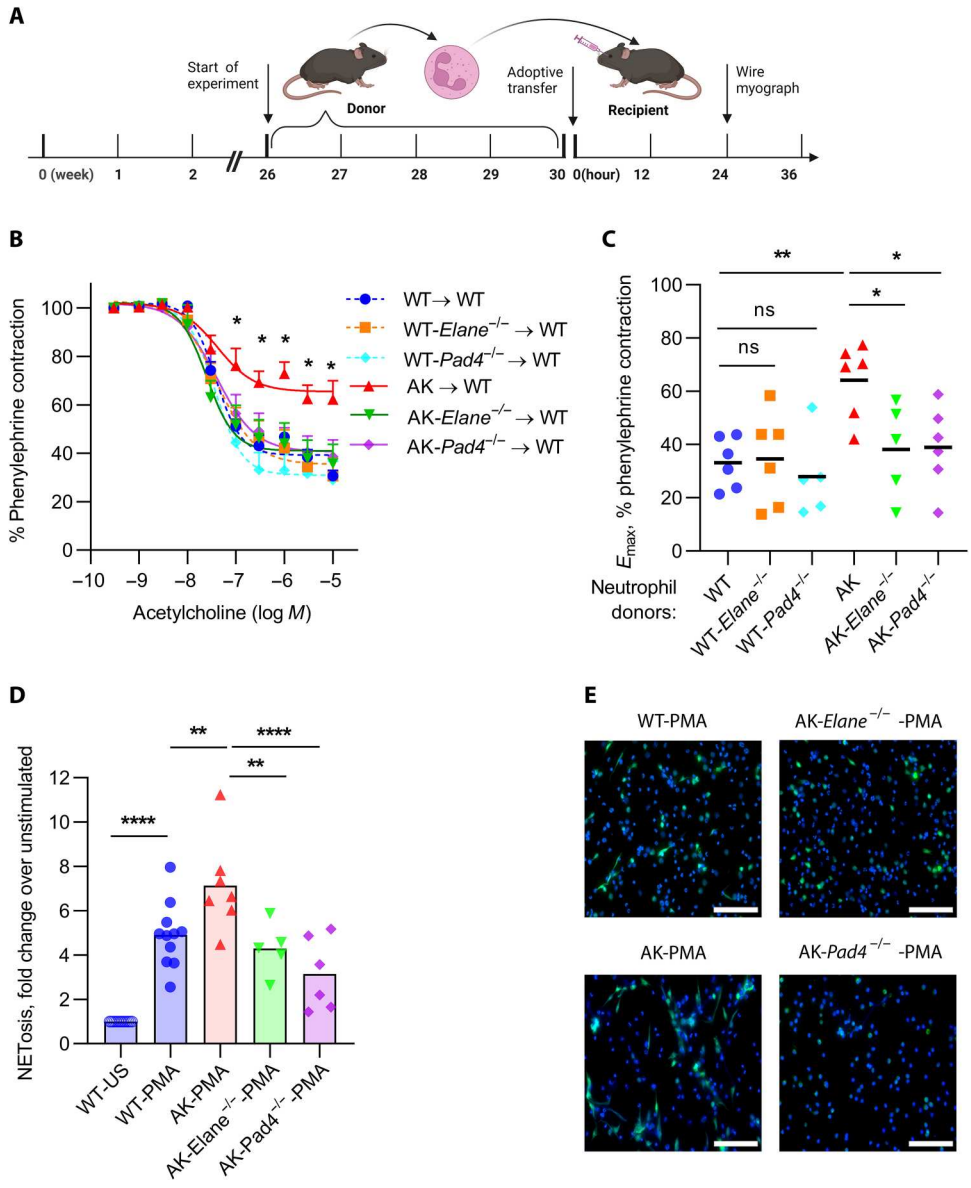

Fig. 5. Impairment of vascular function when aged Akita neutrophils are administered to young WT mice. (**A**) Neutrophils from 26- to 30-week-old mice were transferred to young WT mice. After 24 hours, the aortae of the young mice were tested for vascular dysfunction; schematic prepared with biorender.com. (**B**) Relaxation of aortic rings in response to acetylcholine (Ach) after achieving a stable phenylephrine (PE) contraction plateau. Data are presented relative to the force remaining from the PE contraction, which was set as 100%; means + SEM for $n = 5$ to 6, $^{*}P < 0.05$ Akita neutrophils transfer compared with each other group by two-way ANOVA followed by the Holm-Šídák test. (**C**) E_{max} values as determined by nonlinear regression analysis; mean for $n = 5$ to 6, $^{*}P < 0.05$ and $^{**}P < 0.01$ by one-way ANOVA followed by the Holm-Šídák test. (**D**) Bone marrow neutrophils from the adoptive transfer experiments were also tested for NETosis after PMA stimulation by SYTOX staining; mean for $n = 5$, $^{**}P < 0.01$, $^{***}P < 0.001$, and $^{****}P < 0.0001$ by one-way ANOVA followed by the Holm-Šídák test. (**E**) Representative microscopy indicating NETosis; blue, DNA; green, neutrophil elastase. Scale bars, 100 μm.

also been shown to have a role in pulmonary dysfunction/injuries (*53*) and the destruction of islet cells inherent to the pancreatic origins of type 1 diabetes (*54*). In addition to neutrophils, macrophages may also express neutrophil elastase in atherosclerotic plaques and/or upon stimulation ex vivo (*55*). While some of our data, such as the cell transfer experiments, point to a direct role for neutrophils in diabetic vascular dysfunction, other cells and pathways that interact with neutrophil elastase and PAD4 are likely also deserving of further study.

The intersection of NETs and the vasculature is an area that continues to receive increasing attention. For example, in sepsis, neutrophils engage injured endothelium where they contribute to vascular inflammation via the release of cytokines, ROS, and NETs that support proinflammatory and proangiogenic responses by the endothelium (*56*). We reported previously that NET-derived histones (*57*) can induce endothelial cell activation and venous thrombosis in mice which can be alleviated by neutralizing NETs with defibrotide (a pleiotropic mixture of oligonucleotides)

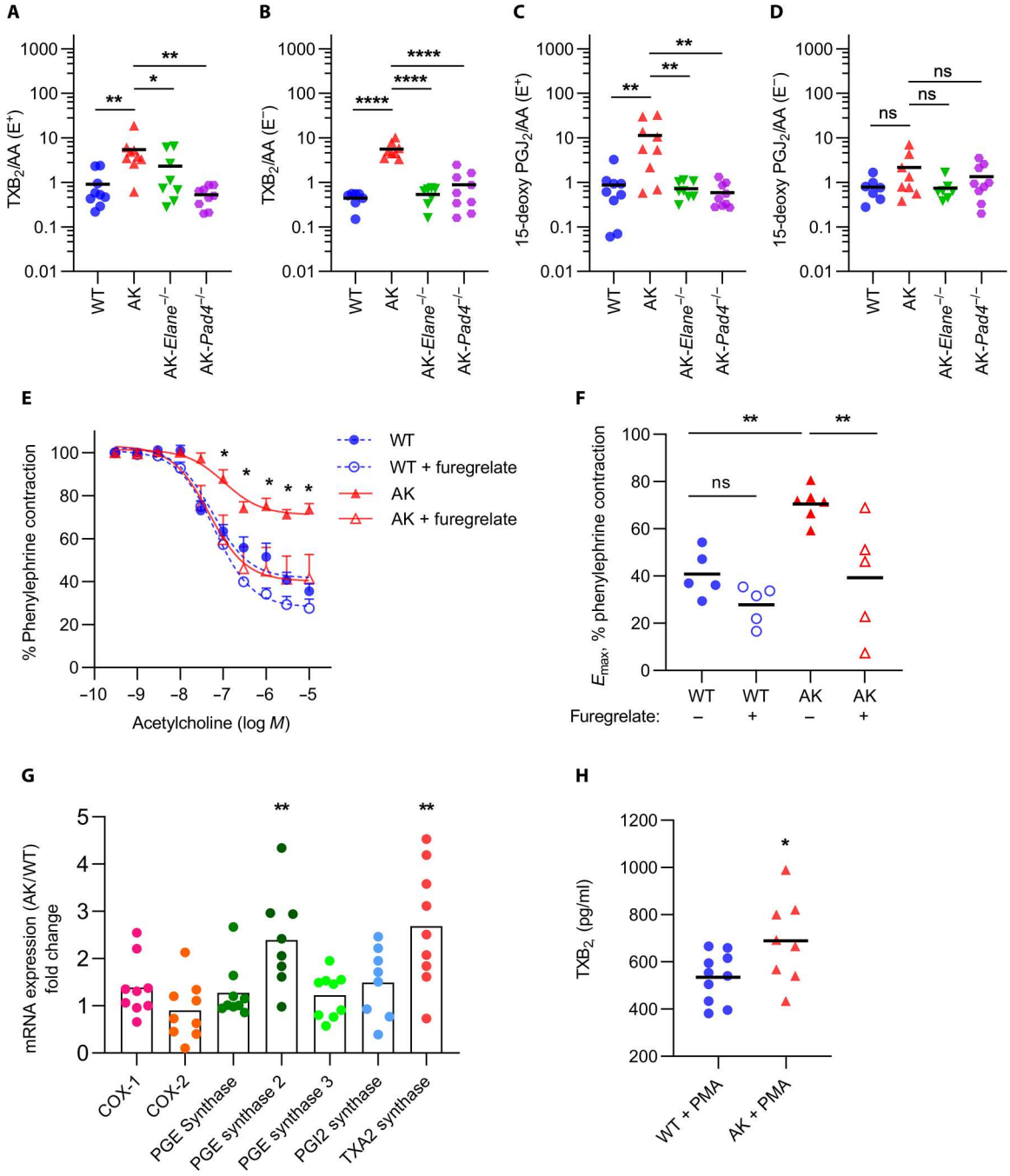

Fig. 6. Thromboxane up-regulation in Akita mice but not in Akita-*Elane*$^{-/-}$ and Akita-*Pad4*$^{-/-}$ mice. Prostanoid metabolites were measured in endothelium-intact (E^+) and endothelium-denuded (E^-) aortae of 24-week-old mice by liquid chromatography/electrospray ionization–tandem mass spectrometry (LC/ESI-MS/MS). The values of prostanoid metabolites detected were all normalized to arachidonic acid (AA) in the aorta. (**A**) TXB_2/AA in intact aortae. (**B**) TXB_2/AA in denuded aortae. (**C**) 15-Deoxy-PGJ_2/AA in intact aortae. (**D**) 15-Deoxy-PGJ_2/AA in denuded aortae. For (A) to (D), mean for $n = 7$ to 9, $^*P < 0.05$, $^{**}P < 0.01$, and $^{****}P < 0.0001$ by one-way ANOVA followed by the Holm-Šídák test. (**E**) Aortic rings from 24-week-old mice were pretreated with furegrelate. Data demonstrate relaxation of aortic rings in response to acetylcholine (Ach) after achieving a stable phenylephrine (PE) contraction plateau. Data are presented relative to the force remaining from the PE contraction, which was set as 100%; mean + SEM for $n = 5$ to 6, $^*P < 0.05$ Akita group compared with Akita + furegrelate group by two-way ANOVA followed by the Holm-Šídák test. (**F**) E_{max} values as determined by nonlinear regression analysis; mean for $n = 5$ to 6, $^{**}P < 0.01$ by one-way ANOVA followed by the Holm-Šídák test. (**G**) Relative mRNA for the indicated genes in bone-marrow neutrophils; mean for $n = 8$ to 9, $^{**}P < 0.01$ Akita neutrophils compared with WT neutrophils by unpaired Student's *t* test. (**H**) TXB_2 levels in bone marrow neutrophil supernatants after stimulating by PMA; mean for $n = 8$ to 10, $^*P < 0.05$ Akita + PMA group compared with WT + PMA group by unpaired Student's *t* test.

(*57*). As a notable recent example, intravascular NETosis appears to be an integral aspect of severe and critical severe acute respiratory syndrome coronavirus 2 (SARS-CoV-2) infection where it contributes to acute respiratory distress syndrome, systemic vascular permeability, and end organ damage (*58*–*60*).

Here, to further investigate the molecular pathways that may mediate the effect of NETosis on vascular dysfunction, we focused on the understudied topic of NETs and their relationship to prostanoids. Prostanoids are important regulators of vessel tone. Arachidonic acid (AA) is processed via cyclooxygenase to produce prostaglandin (PG)G_2, the precursor of PGH_2. PGH_2 is then converted into various vasoactive prostanoids, including TXA_2, $PGF_{2\alpha}$, PGE_2, PGD_2, PGI_2, and various downstream metabolites. We discovered that among these prostanoids, the TXB_2/AA ratio was strongly up-regulated in both endothelium-intact and endothelium-denuded Akita aortae, an effect that was reversed in NETosis-deficient Akita mice. Together, these data suggest that TXA_2 derived from a source external to the endothelium and related to NETosis impairs the vasodilatory response of Akita mice. While platelets, including platelet-derived microvesicles (*61*–*63*), are the best-known source of TXA_2, it can also be produced by other cells including endothelial cells (*64*, *65*), smooth muscle cells (*66*), and inflammatory cells (*30*–*32*). In Akita mice, the increase in TXA_2 appeared to be NETosis-dependent and derived from a source external to the endothelium. We can speculate that the TXA_2 is produced either by neutrophils themselves during the process of NETosis or potentially by VSMCs in response to NETosis. While the release of TXA_2 by VSMCs has not been extensively studied, there are more data to support its release by neutrophils. For example, sheep neutrophils produce TXA_2 after stimulation by thrombin (*67*) or complement (*68*). Mouse neutrophils may also produce TXA_2 to modulate their own migration to draining nodes (*32*). The release of TXA_2 by rat lung neutrophils has been shown to be strongly up-regulated by selenium deficiency (*69*). Furthermore, human neutrophils can release 8- to 20-fold higher TXA_2 after stimulation by calcimycin (A23187) and other proinflammatory factors (*67*), while human neutrophils exposed to conditions reminiscent of preeclampsia release TXA_2 and tumor necrosis factor–α that trigger vascular inflammation (*31*). Although our study suggests that the origin of the TXA_2 may be partially from hyperactive neutrophils, lineage-specific knockout mice will likely be needed to fully elicit the origins of thromboxanes in diabetic vessel walls.

Beyond TXA_2, we found that 15-deoxy-PGJ_2 was up-regulated in the endothelium of aged Akita aortae. This prostanoid was the first endogenous ligand of PPAR-γ to be discovered and has been reported to have anti-inflammatory and antioxidative roles in many different tissues (*70*). At the same time, others have reported PPAR-γ–independent actions of 15-deoxy-PGJ_2 on human umbilical vein endothelial cells (*71*). For now, our hypothesis is that 15-deoxy-PGJ_2 is up-regulated as an attempted compensatory mechanism against vascular dysfunction. 15-Deoxy-PGJ_2 suppresses transcription of the human TXA_2 receptor gene through PPAR-γ in human erythroleukemia cells in vitro (*72*), while the PPAR-γ agonist, pioglitazone, increases myosin light chain phosphatase activity, desensitizing the vascular smooth muscle to agonist signaling in primary rat aortic VSMCs (*73*), but whether there is an actual biological impact of 15-deoxy-PGJ_2 on the diabetic aorta remains unclear. We reported strong endothelial dysfunction but slight smooth muscle dysfunction in intact Akita mice aortae by wire myography, in which the 15-deoxy-PGJ2 may have already, to some extent, relieved the smooth muscle dysfunction. To shed light on the potential role of 15-deoxy-PGJ_2 in masking smooth muscle dysfunction, further vascular function studies using endothelium-denuded aortae may be needed.

In summary, this study suggests that NETosis is a contributor to the preclinical vascular dysfunction of type 1 diabetic mice. Future studies should ask whether inhibition of NETosis is also fruitful in models equipped to assess more mature phenotypes such as diabetes-accelerated frank atherosclerosis, as well as the extent to which the findings of this study would extend to models of type 2 diabetes. Because Akita mice are known to develop some microvascular manifestations of diabetes, such as nephropathy (*74*–*76*), we should be well positioned in the future to determine the extent to which NETosis affects diabetic kidney and possibly retinal disease. We believe that studies should also continue to interrogate the interesting and pharmacologically relevant intersection of neutrophils and prostanoids.

MATERIALS AND METHODS

Mice

All mouse experiments were performed in accordance with the University of Michigan Institutional Animal Care and Use Committee guidelines. Mice were housed in a designated pathogen-free barrier facility and were fed with standard chow unless otherwise indicated. C57BL/6J (WT), heterozygous C57BL/6-*Ins2*^{Akita}/J (Akita), and B6.129X1-*Elane*^{tm1Sds}/J (*Elane*$^{-/-}$) mice were originally purchased from the Jackson Laboratory. *PAD4* knockout mice (*PAD4*$^{-/-}$) (*26*) were backcrossed for 10 generations onto the C57BL/6J background before their use in these studies. Only male C57BL/6J-*Ins2*$^{+/Akita}$ mice were used for experiments given the known increased penetrance of the diabetic phenotype for males in this model (*77*, *78*).

Plasma glucose quantification

The plasma glucose levels in diabetic and nondiabetic mice were measured by the University of Michigan In-Vivo Animal Core (IVAC) facility using Glucose Hexokinase (Liquid) Reagent (AMS Diagnostics) run on a Liasys 330 Clinical Chemistry System (AMS Diagnostics) as per the manufacturer's instructions.

Vascular functional assays

Vascular function experiments were performed as previously described (*29*). Briefly, mice were anesthetized with pentobarbital (80 mg/kg, intraperitoneally), and aortae were carefully dissected and cleaned to remove any adherent fat tissue. Each thoracic aorta was gently perfused with 1× phosphate-buffered saline (PBS) to remove any residual blood and cut into two equal halves. One-half of the aorta was additionally perfused with 0.1% Triton X-100 in PBS to remove the endothelium (endothelium-denuded), while the endothelium was left intact in the other half. Both the intact and denuded aortae were cut into 2-mm rings and mounted in a myograph bath chamber (DMT wire myograph) containing warmed (37°C) physiological saline solution (PSS; 130 mM NaCl, 4.7 mM KCl, 1.18 mM KH_2PO_4, 1.17 mM $MgSO_4$ $7H_2O$, 14.9 mM $NaHCO_3$, 5.5 mM glucose, 0.026 mM EDTA, and 1.6 mM $CaCl_2$) and bubbled continuously with 95% O_2 and 5% CO_2 mixture (pH 7.4). Rings were set at a passive tension of 700 mg

and equilibrated for 30 min. Simultaneously, both the intact and denuded aortae were snap-frozen and stored in a −80°C freezer for further analysis. Following equilibration, rings were exposed to high potassium PSS as described previously (*79*). KPSS was removed by washing the rings five times with PSS (10 min for each wash). Rings were contracted with PE at a final concentration of 0.3 μM, and endothelium-mediated relaxation was determined as a measure of the concentration-response curve when exposed to cumulative concentrations of acetylcholine (10^{-9} to 10^{-5} M). To measure the endothelium-independent vascular smooth muscle relaxation, U46619-precontracted aortic rings (final concentration, 2.6 nM) were exposed to cumulative concentrations of sodium nitroprusside (10^{-10} to 10^{-6} M). Relaxation was reported as the force remaining at each dose of either acetylcholine or sodium nitroprusside and expressed as the percentage of the force at the plateau generated by either PE or U46619, respectively. To assess the effect of thromboxane on endothelium intact relaxation, aortic rings were preincubated with a known thromboxane synthase inhibitor: furegrelate (Cayman Chemical) at a final concentration of 10 μM, followed by PE contraction and acetylcholine relaxation, as described above.

Quantification of MPO-DNA complexes

MPO-DNA complexes were quantified as described previously (*80*) with minor modifications. Briefly, a high-binding EIA/RIA 96-well plate (Costar) was coated overnight at 4°C with anti-MPO antibody (Bio-Rad) diluted to a final concentration of 0.5 μg/ml in coating buffer (Cell Death Detection ELISA Kit, MilliporeSigma). The plate was washed three times with wash buffer (0.05% Tween-20 in PBS) and blocked with 4% bovine serum albumin (MilliporeSigma) for 90 min at room temperature. The plate was washed again with the wash buffer before incubating for 90 min at room temperature with mouse plasma samples diluted in blocking buffer (1:250). The plate was washed with the wash buffer and incubated for an hour at room temperature with 10× anti-DNA antibody (Cell Death Detection ELISA Kit; MilliporeSigma), diluted 1:100 in blocking buffer. The plate was washed before developing the plate with 3,3′,5,5′-tetramethylbenzidine substrate (Invitrogen, Thermo Fisher Scientific). The reaction was stopped by the addition of 1 M sulfuric acid stop solution, and the absorbance was measured at a wavelength of 450 nm using a Cytation 5 Cell Imaging Multi-Mode Reader (BioTek).

Soluble ICAM-1 enzyme-linked immunosorbent assay

Soluble ICAM-1 levels in plasma were quantified using enzyme-linked immunosorbent assay (ELISA; DY796, R&D systems) according to the manufacturer's instructions.

Mouse neutrophil purification

Bone marrow from femurs and tibias was collected, and neutrophils were purified using Mouse Neutrophil Enrichment Kit (STEMCELL Technologies) according to the manufacturer's instructions. For peritoneal neutrophils, peritonitis was induced by infusing 1 ml of aged 3% Brewer thioglycolate medium (Fisher Scientific), via intraperitoneal injection. Peritoneal lavage was collected 16 hours after infusion by injecting 10 ml of ice-cold PBS supplemented with EDTA at a final concentration of 5 mM. Cells were pelleted by centrifugation at 500*g* at room temperature for 10 min. Neutrophils were isolated using the Mouse Neutrophil Enrichment Kit as per the manufacturer's instructions.

Seahorse extracellular flux assay

Extracellular flux analysis was performed at 37°C without CO_2 using the XFe96 Seahorse Extracellular Flux Analyzer (Agilent). For all Seahorse experiments, XF RPMI, medium supplements, and stress test reagents were purchased from Agilent. Neutrophils (2×10^5 per well) isolated from peritoneal lavage were plated on 0.001% poly-L-lysine (Sigma-Aldrich)–coated Seahorse culture plates in XF RPMI. For the glycolysis stress test, the medium was supplemented with 2 mM glutamine; then, cells were serially treated with 10 mM glucose, 2 mM oligomycin, and 50 mM 2-deoxyglucose (2-DG) according to the standard stress test protocol provided by Agilent. For the mitochondrial stress test, the medium was supplemented with 2 mM glutamine, 10 mM glucose, and 1 mM pyruvate, and then, cells were serially treated with 2 mM oligomycin, 2 mM carbonyl cyanide *p*-trifluoromethoxyphenylhydrazone (FCCP), and 0.5 mM rotenone/antimycin A (Rot/AA) according to the standard stress test protocol provided by Agilent. For some experiments, baseline extracellular acidification rate (ECAR) and oxygen consumptoin rate (OCR) were measured for 3 cycles (18 min); then, neutrophils were treated with stimulants (PMA; 250 nM), and changes in ECAR and OCR were measured over 4 hours.

NETosis assays

A total of 2×10^5 mouse bone marrow or peritoneal neutrophils were resuspended in RPMI supplemented with L-glutamine, 1% fetal bovine serum (FBS), and SYTOX green (Thermo Fisher Scientific) to a final concentration of 250 nM. Cells were incubated with 250 nM PMA for 20 hours at 37°C and 5% CO_2. Following incubation, culture media was slowly removed, and cells were washed twice with 1x PBS. SYTOX fluorescence was measured at excitation and emission wavelengths of 504 nm and 523 nm using a Cytation 5 Cell Imaging Multi-Mode Reader (BioTek).

Immunofluorescence microscopy

Bone marrow (2×10^5) or peritoneal neutrophils (2×10^5) were resuspended in RPMI supplemented with L-glutamine (Gibco) and 1% FBS (Gibco) and were seeded onto 0.001% poly-L-lysine–coated coverslips. The NET formation was induced by incubating the cells in the presence of 250 nM PMA (Sigma-Aldrich) for 20 hours at 37°C and 5% CO_2. Following stimulation, cells were fixed with 4% paraformaldehyde (PFA; Sigma-Aldrich) for 10 min at room temperature, followed by overnight blocking in 10% FBS in PBS (Gibco). Fixed cells were incubated with polyclonal antibody to anti–histone H3 (Abcam, Ab5103) in blocking buffer for 1 hour at 4°C, followed by fluorescein isothiocyanate (FITC)–conjugated secondary (Southern Biotech) for 1 hour at 4°C. Nuclear DNA was detected with Hoechst 33342. Coverslips were mounted with ProLong Gold Antifade (Thermo Fisher Scientific), and images were collected with a Cytation 5 Cell Imaging Multi-Mode Reader (BioTek).

Generation of Akita-*Elane*$^{-/-}$ and Akita-*Pad4*$^{-/-}$ mice

Male $Ins2^{+/Akita}$ mice were crossed with female *Elane*$^{-/-}$ mice to generate double heterozygotes: $Ins2^{+/Akita}$-*Elane*$^{+/-}$. Male double

heterozygotes from the F1 generation were crossed again with female *Elane*$^{-/-}$ to generate the diabetic experimental mice: Ins2$^{+/Akita}$-*Elane*$^{-/-}$. The experimental mice were maintained by crossing male Ins2$^{+/Akita}$-*Elane*$^{-/-}$ mice with female *Elane*$^{-/-}$ mice, where half the progeny were diabetic experimental mice, and another half were nondiabetic experimental controls. Ins2$^{+/Akita}$-*PAD4*$^{-/-}$ mice were also generated using a similar approach.

In vivo drug study

To assess the role of NETs on vascular dysfunction, 24-week-old mice were fed with either standard base chow (8604-Envigo) or GW311616A (Alfa Chemistry), incorporated into 8604 base chow (Envigo), and dosed at 2.2 mg/kg per day for 5 weeks (*21*). Briefly, GW311616A was added to the base chow and blended thoroughly in a mixer. Water was added to the mixture and mixed for an additional 10 min before being pressed into pellets. To remove the added water, pellets were dried at 50°C for 8 hours and subsequently cooled down.

Neutrophil adoptive transfer

Purified bone marrow neutrophils from the donor mice were resuspended in 0.9% sodium chloride solution-USP grade (Fisher Scientific), and 7×10^6 neutrophils were administered to the recipient mice via retro-orbital injection. Mice were humanely euthanized, and vascular function was assessed 24 hours after adoptive transfer.

Isolation of platelets from murine blood

Briefly, mice were anesthetized with isoflurane, and blood was collected by cardiac puncture. Blood was immediately mixed with acid citrate dextrose (1.5% citric acid, 2.5% trisodium citrate, and 2% dextrose) solution at 9 to 1 ratio and further diluted three to four times with modified Tyrode's buffer [134 mM NaCl, 2.9 mM KCl, 0.34 mM Na_2HPO_4, 12 mM $NaHCO_3$, 20 mM Hepes, 1.0 mM $MgCl_2$, 5.0 mM glucose, and 0.35% bovine serum albumin (pH 7.35)]. Whole blood was centrifuged at 100*g*, without brake, for 15 min at room temperature. Platelet-rich plasma (PRP) was carefully collected, and to inhibit platelet activation, prostaglandin E1 (1 μM) was added immediately. PRP samples were centrifuged at 700*g* for 6 min to obtain platelet pellets. Pellets were then washed with modified Tyrode's buffer in the presence of prostaglandin E1 (1 μM) and lastly resuspended in modified Tyrode's buffer.

Flow cytometry

Briefly, purified bone marrow neutrophils from 24-week-old C57BL/6 mice were incubated with a mouse Fc-receptor blocker (BioLegend) and stained with fluorescently conjugated antibody against CD41 (FITC-conjugated anti-CD41, BioLegend) for 20 min at room temperature. Cells were washed twice with flow buffer (1× PBS, supplemented with 1% FBS and 5 mM EDTA) and fixed with 2% PFA (Fisher). As a positive control, mouse platelets were purified from the whole blood and stained as aforementioned. Samples were analyzed on a BioRad-ZE5 flow cytometer. Further data analysis was done using FlowJo (Tree Star) software.

Quantitative polymerase chain reaction

RNA from mouse bone marrow neutrophils was isolated using a Direct Zol RNA Purification kit (Zymo Research), according to the manufacturer's instructions. cDNA synthesis and quantitative polymerase chain reaction (qPCR) were performed as described previously (*57*). mRNA expression levels were normalized to β-actin. All gene primers were purchased from Sigma-Aldrich (KiCqStart).

Quantification of TXB_2

Bone marrow neutrophils (0.5×10^6) were resuspended in RPMI supplemented with L-glutamine and 1% FBS and stimulated in the presence or absence of 250 nM PMA for 8 hours at 37°C and 5% CO_2. Following incubation, the culture supernatant was collected and centrifuged at 450*g* at room temperature for 10 min to remove any contaminated cells. Cell-free supernatant was collected and immediately frozen at −80°C until further analysis. TXB_2 levels in the supernatant were measured using the TXB_2 ELISA kit (Cayman Chemical) according to the manufacturer's instructions.

Identification and quantification of prostanoid metabolites

To elucidate the role of cyclooxygenase-generated prostanoids on vascular dysfunction in diabetic mice, levels of these vasoactive metabolites were quantified by liquid chromatography/electrospray ionization–tandem mass spectrometry in multiple reaction monitoring modes as described previously (*81*). Authentic prostaglandins, their precursor, and their deuterium-labeled analogs were purchased from Cayman Chemical. Briefly, frozen aorta samples (endothelium intact and endothelium-denuded) were thawed and homogenized in 500 μl of PBS supplemented with butylated hydroxytoluene (100 μM) and diethylenetriaminepentaacetic acid (1 μM, pH 7), followed by the addition of deuterium-labeled (200 pM for prostanoids and 5 nM for their precursor per sample) internal standard cocktail. Samples were further incubated with an excess amount of sodium borohydride for 5 min before subjecting to base hydrolysis with potassium hydroxide (1 M) in methanol under nitrogen for 1 hour at 40°C. The reaction was terminated by the addition of 10% acetic acid (2 ml). Lipids were extracted with chloroform/ethyl acetate (4:1, v/v) and centrifuged (4000 rpm for 30 min) twice, and the organic layers were pooled, dried, and stored at −80°C for further processing. Samples were reconstituted in an acetonitrile/water/acetic acid (40:60:0.02, v/v/v) mixture, and liquid chromatography separations were performed using Reversed Phase Luna C18 LC column (100 Å, 3 μm, 150 mm by 2 mm; Phenomenex Inc., Torrance, CA) on Agilent 1200 LC system coupled with Agilent 6490 Triple Quadrupole system mass spectrometer (Santa Clara, CA). Analytes were detected in negative mode, and prostaglandins and their precursor were identified on the basis of the compound-specific retention times and unique MS fragmentation patterns and further quantified by comparing peak areas of the analyte of interest and their corresponding isotopically labeled internal standards.

Statistical analysis

For wire myography, the difference between each group in two-group or multigroup comparison was evaluated using two-way analysis of variance (ANOVA) followed by the Holm-Šídák test. The E_{max} values were calculated with nonlinear regression analysis by GraphPad Prism software and were compared by unpaired Student's *t* test between two groups or one-way ANOVA followed by the Holm-Šídák test between selected pairs of groups in multigroup comparison. For glucose test, MPO-DNA complexes, the Seahorse experiments, NETosis assays, prostanoid metabolite determination,

qPCR analysis, and TXB_2 assay, differences in values between two groups were compared by unpaired Student's *t* test, and the difference between selected pairs of groups in multigroup comparison was evaluated using one-way ANOVA followed by the Holm-Šídák test.

Supplementary Materials

This PDF file includes:

Figs. S1 to S7

REFERENCES AND NOTES

1. S. Jakobsson, L. Bergström, F. Björklund, T. Jernberg, L. Söderström, T. Mooe, Risk of ischemic stroke after an acute myocardial infarction in patients with diabetes mellitus. *Circ. Cardiovasc. Qual. Outcomes* **7**, 95–101 (2014).
2. W. Fan, Epidemiology in diabetes mellitus and cardiovascular disease. *Cardiovasc. Endocrinol.* **6**, 8–16 (2017).
3. M. J. Fowler, Microvascular and macrovascular complications of diabetes. *Clin. Diabetes.* **29**, 116–122 (2011).
4. J. Calles-Escandon, M. Cipolla, Diabetes and endothelial dysfunction: a clinical perspective. *Endocr. Rev.* **22**, 36–52 (2001).
5. V. Brinkmann, U. Reichard, C. Goosmann, B. Fauler, Y. Uhlemann, D. S. Weiss, Y. Weinrauch, A. Zychlinsky, Neutrophil extracellular traps kill bacteria. *Science* **303**, 1532–1535 (2004).
6. L. Menegazzo, S. Ciciliot, N. Poncina, M. Mazzucato, M. Persano, B. Bonora, M. Albiero, S. Vigili de Kreutzenberg, A. Avogaro, G. P. Fadini, NETosis is induced by high glucose and associated with type 2 diabetes. *Acta Diabetol.* **52**, 497–503 (2015).
7. Y. Wang, Y. Xiao, L. Zhong, D. Ye, J. Zhang, Y. Tu, S. R. Bornstein, Z. Zhou, K. S. L. Lam, A. Xu, Increased neutrophil elastase and proteinase 3 and augmented NETosis are closely associated with β-cell autoimmunity in patients with type 1 diabetes. *Diabetes* **63**, 4239–4248 (2014).
8. T. A. Fuchs, U. Abed, C. Goosmann, R. Hurwitz, I. Schulze, V. Wahn, Y. Weinrauch, V. Brinkmann, A. Zychlinsky, Novel cell death program leads to neutrophil extracellular traps. *J. Cell Biol.* **176**, 231–241 (2007).
9. S. L. Wong, D. D. Wagner, Peptidylarginine deiminase 4: A nuclear button triggering neutrophil extracellular traps in inflammatory diseases and aging. *FASEB J.* **32**, fj201800691R (2018).
10. M. J. Kaplan, M. Radic, Neutrophil extracellular traps: Double-edged swords of innate immunity. *J. Immunol.* **189**, 2689–2695 (2012).
11. R. Njeim, W. S. Azar, A. H. Fares, S. T. Azar, H. Kfoury Kassouf, A. A. Eid, NETosis contributes to the pathogenesis of diabetes and its complications. *J. Mol. Endocrinol.* **65**, R65–R76 (2020).
12. L. Wang, X. Zhou, Y. Yin, Y. Mai, D. Wang, X. Zhang, Hyperglycemia induces neutrophil extracellular traps formation through an NADPH oxidase-dependent pathway in diabetic retinopathy. *Front. Immunol.* **9**, 3076 (2018).
13. S. L. Wong, M. Demers, K. Martinod, M. Gallant, Y. Wang, A. B. Goldfine, C. R. Kahn, D. D. Wagner, Diabetes primes neutrophils to undergo NETosis, which impairs wound healing. *Nat. Med.* **21**, 815–819 (2015).
14. M. B. Joshi, G. Baipadithaya, A. Balakrishnan, M. Hegde, M. Vohra, R. Ahamed, S. K. Nagri, L. Ramachandra, K. Satyamoorthy, Elevated homocysteine levels in type 2 diabetes induce constitutive neutrophil extracellular traps. *Sci. Rep.* **6**, 36362 (2016).
15. A. Carestia, G. Frechtel, G. Cerrone, M. A. Linari, C. D. Gonzalez, P. Casais, M. Schattner, NETosis before and after hyperglycemic control in type 2 diabetes mellitus patients. *PLOS ONE* **11**, e0168647 (2016).
16. R. J. Roth Flach, M. P. Czech, NETs and traps delay wound healing in diabetes. *Trends Endocrinol. Metab.* **26**, 451–452 (2015).
17. G. P. Fadini, L. Menegazzo, M. Rigato, V. Scattolini, N. Poncina, A. Bruttocao, S. Ciciliot, F. Mammano, C. D. Ciubotaru, E. Brocco, M. C. Marescotti, R. Cappellari, G. Arrigoni, R. Millioni, S. Vigili de Kreutzenberg, M. Albiero, A. Avogaro, NETosis delays diabetic wound healing in mice and humans. *Diabetes* **65**, 1061–1071 (2016).
18. V. Brinkmann, A. Zychlinsky, Neutrophil extracellular traps: Is immunity the second function of chromatin? *J. Cell Biol.* **198**, 773–783 (2012).
19. J. Cools-Lartigue, J. Spicer, B. McDonald, S. Gowing, S. Chow, B. Giannias, F. Bourdeau, P. Kubes, L. Ferri, Neutrophil extracellular traps sequester circulating tumor cells and promote metastasis. *J. Clin. Invest.* **123**, 3446–3458 (2013).
20. F. von Nussbaum, V. M. J. Li, Neutrophil elastase inhibitors for the treatment of (cardio)-pulmonary diseases: Into clinical testing with pre-adaptive pharmacophores. *Bioorg. Med. Chem. Lett.* **25**, 4370–4381 (2015).
21. G. Wen, W. An, J. Chen, E. M. Maguire, Q. Chen, F. Yang, S. W. A. Pearce, M. Kyriakides, L. Zhang, S. Ye, S. Nourshargh, Q. Xiao, Genetic and pharmacologic inhibition of the neutrophil elastase inhibits experimental atherosclerosis. *J. Am. Heart Assoc.* **7**, 1–29 (2018).
22. J. S. Knight, W. Luo, A. A. O'Dell, S. Yalavarthi, W. Zhao, V. Subramanian, C. Guo, R. C. Grenn, P. R. Thompson, D. T. Eitzman, M. J. Kaplan, Peptidylarginine deiminase inhibition reduces vascular damage and modulates innate immune responses in murine models of atherosclerosis. *Circ. Res.* **114**, 947–956 (2014).
23. J. S. Knight, W. Zhao, W. Luo, V. Subramanian, A. A. O'Dell, S. Yalavarthi, J. B. Hodgin, D. T. Eitzman, P. R. Thompson, M. J. Kaplan, Peptidylarginine deiminase inhibition is immunomodulatory and vasculoprotective in murine lupus. *J. Clin. Invest.* **123**, 2981–2993 (2013).
24. J. S. Knight, V. Subramanian, A. A. O'Dell, S. Yalavarthi, W. Zhao, C. K. Smith, J. B. Hodgin, P. R. Thompson, M. J. Kaplan, Peptidylarginine deiminase inhibition disrupts NET formation and protects against kidney, skin and vascular disease in lupus-prone MRL/lpr mice. *Ann. Rheum. Dis.* **74**, 2199–2206 (2015).
25. H. Wang, Q. Wang, J. Venugopal, J. Wang, K. Kleiman, C. Guo, D. T. Eitzman, Obesity-induced endothelial dysfunction is prevented by neutrophil extracellular trap inhibition. *Sci. Rep.* **8**, 4881 (2018).
26. P. Li, M. Li, M. R. Lindberg, M. J. Kennett, N. Xiong, Y. Wang, PAD4 is essential for antibacterial innate immunity mediated by neutrophil extracellular traps. *J. Exp. Med.* **207**, 1853–1862 (2010).
27. A. J. Monteith, J. M. Miller, C. N. Maxwell, W. J. Chazin, E. P. Skaar, Neutrophil extracellular traps enhance macrophage killing of bacterial pathogens. *Sci. Adv.* **7**, eabj2101 (2021).
28. G. Franck, T. L. Mawson, E. J. Folco, R. Molinaro, V. Ruvkun, D. Engelbertsen, X. Liu, Y. Tesmenitsky, E. Shvartz, G. K. Sukhova, J.-B. Michel, A. Nicoletti, A. Lichtman, D. Wagner, K. J. Croce, P. Libby, Roles of PAD4 and NETosis in experimental atherosclerosis and arterial injury: Implications for superficial erosion. *Circ. Res.* **123**, 33–42 (2018).
29. H. A. Toque, K. P. Nunes, L. Yao, Z. Xu, D. Kondrikov, Y. Su, R. C. Webb, R. B. Caldwell, R. W. Caldwell, Akita spontaneously type 1 diabetic mice exhibit elevated vascular arginase and impaired vascular endothelial and nitrergic function. *PLOS ONE* **8**, e72277 (2013).
30. P. M. O'Byrne, *Prostanoids in Asthma and COPD* (Elsevier, 2009), pp. 275–282.
31. J. E. Vaughan, S. W. Walsh, Neutrophils from pregnant women produce thromboxane and tumor necrosis factor-alpha in response to linoleic acid and oxidative stress. *Am. J. Obstet. Gynecol.* **193**, 830–835 (2005).
32. C.-W. Yang, E. R. Unanue, Neutrophils control the magnitude and spread of the immune response in a thromboxane A2-mediated process. *J. Exp. Med.* **210**, 375–387 (2013).
33. X. Fang, L. Ma, Y. Wang, F. Ren, Y. Yu, Z. Yuan, H. Wei, H. Zhang, Y. Sun, Neutrophil extracellular traps accelerate vascular smooth muscle cell proliferation via Akt/CDKN1b/TK1 accompanying with the occurrence of hypertension. *J. Hypertens.* **40**, 2045–2057 (2022).
34. L. Kang, H. Yu, X. Yang, Y. Zhu, X. Bai, R. Wang, Y. Cao, H. Xu, H. Luo, L. Lu, M.-J. Shi, Y. Tian, W. Fan, B.-Q. Zhao, Neutrophil extracellular traps released by neutrophils impair revascularization and vascular remodeling after stroke. *Nat. Commun.* **11**, 2488 (2020).
35. Y. Zhou, W. Tao, F. Shen, W. Du, Z. Xu, Z. Liu, The emerging role of neutrophil extracellular traps in arterial, venous and cancer-associated thrombosis. *Front. Cardiovasc. Med.* **8**, 786387 (2021).
36. L. P. Blanco, X. Wang, P. M. Carlucci, J. J. Torres-Ruiz, J. Romo-Tena, H. Sun, M. Hafner, M. J. Kaplan, RNA externalized by neutrophil extracellular traps promotes inflammatory pathways in endothelial cells. *Arthritis Rheumatol.* **73**, 2282–2292 (2021).
37. J. S. Knight, Y. Kanthi, Mechanisms of immunothrombosis and vasculopathy in antiphospholipid syndrome. *Semin. Immunopathol.* **44**, 347–362 (2022).
38. Y. Zuo, M. Zuo, S. Yalavarthi, K. Gockman, J. A. Madison, H. Shi, W. Woodard, S. P. Lezak, N. L. Lugogo, J. S. Knight, Y. Kanthi, Neutrophil extracellular traps and thrombosis in COVID-19. *J. Thromb. Thrombolysis* **51**, 446–453 (2021).
39. S. K. Popp, F. Vecchio, D. J. Brown, R. Fukuda, Y. Suzuki, Y. Takeda, R. Wakamatsu, M. A. Sarma, J. Garrett, A. Giovenzana, E. Bosi, A. R. A. Lafferty, K. J. Brown, E. E. Gardiner, L. A. Coupland, H. E. Thomas, B. H. Chong, C. R. Parish, M. Battaglia, A. Petrelli, C. J. Simeonovic, Circulating platelet-neutrophil aggregates characterize the development of type 1 diabetes in humans and NOD mice. *JCI insight.* **7**, e153993 (2022).
40. Y. Garciafigueroa, B. E. Phillips, C. Engman, M. Trucco, N. Giannoukakis, Neutrophil-associated inflammatory changes in the pre-diabetic pancreas of early-age NOD mice. *Front. Endocrinol.(Lausanne)* **12**, 565981 (2021).
41. J.-H. Jeon, C.-W. Hong, E. Y. Kim, J. M. Lee, Current understanding on the metabolism of neutrophils. *Immune Netw.* **20**, e46 (2020).
42. O. Rodríguez-Espinosa, O. Rojas-Espinosa, M. M. B. Moreno-Altamirano, E. O. López-Villegas, F. J. Sánchez-García, Metabolic requirements for neutrophil extracellular traps formation. *Immunology* **145**, 213–224 (2015).
43. E. P. Azevedo, N. C. Rochael, A. B. Guimarães-Costa, T. S. de Souza-Vieira, J. Ganilho, E. M. Saraiva, F. L. Palhano, D. Foguel, A metabolic shift toward pentose phosphate

pathway is necessary for amyloid fibril- and phorbol 12-myristate 13-acetate-induced neutrophil extracellular trap (NET) formation. *J. Biol. Chem.* **290**, 22174–22183 (2015).
44. T. Chen, Y. Li, R. Sun, H. Hu, Y. Liu, M. Herrmann, Y. Zhao, L. E. Muñoz, Receptor-mediated NETosis on neutrophils. *Front. Immunol.* **12**, 775267 (2021).
45. K. D. Metzler, T. A. Fuchs, W. M. Nauseef, D. Reumaux, J. Roesler, I. Schulze, V. Wahn, V. Papayannopoulos, A. Zychlinsky, Myeloperoxidase is required for neutrophil extracellular trap formation: Implications for innate immunity. *Blood* **117**, 953–959 (2011).
46. V. Papayannopoulos, K. D. Metzler, A. Hakkim, A. Zychlinsky, Neutrophil elastase and myeloperoxidase regulate the formation of neutrophil extracellular traps. *J. Cell Biol.* **191**, 677–691 (2010).
47. T. M. Chamardani, S. Amiritavassoli, Inhibition of NETosis for treatment purposes: Friend or foe? *Mol. Cell. Biochem.* **477**, 673–688 (2022).
48. X. Zhao, L. Yang, N. Chang, L. Hou, X. Zhou, L. Yang, L. Li, Neutrophils undergo switch of apoptosis to NETosis during murine fatty liver injury via S1P receptor 2 signaling. *Cell Death Dis.* **11**, 379 (2020).
49. M. Dubey, S. Nagarkoti, D. Awasthi, A. K. Singh, T. Chandra, J. Kumaravelu, M. K. Barthwal, M. Dikshit, Nitric oxide-mediated apoptosis of neutrophils through caspase-8 and caspase-3-dependent mechanism. *Cell Death Dis.* **7**, e2348 (2016).
50. S. J. F. Macdonald, M. D. Dowle, L. A. Harrison, P. Shah, M. R. Johnson, G. G. A. Inglis, G. D. E. Clarke, R. A. Smith, D. Humphreys, C. R. Molloy, A. Amour, M. Dixon, G. Murkitt, R. E. Godward, T. Padfield, T. Skarzynski, O. M. P. Singh, K. A. Kumar, G. Fleetwood, S. T. Hodgson, G. W. Hardy, H. Finch, The discovery of a potent, intracellular, orally bioavailable, long duration inhibitor of human neutrophil elastase—GW311616A a development candidate. *Bioorg. Med. Chem. Lett.* **11**, 895–898 (2001).
51. N. Aikawa, A. Ishizaka, H. Hirasawa, S. Shimazaki, Y. Yamamoto, H. Sugimoto, M. Shinozaki, N. Taenaka, S. Endo, T. Ikeda, Y. Kawasaki, Reevaluation of the efficacy and safety of the neutrophil elastase inhibitor, Sivelestat, for the treatment of acute lung injury associated with systemic inflammatory response syndrome; a phase IV study. *Pulm. Pharmacol. Ther.* **24**, 549–554 (2011).
52. D. Zhu, Y. Lu, Y. Wang, Y. Wang, PAD4 and its inhibitors in cancer progression and prognosis. *Pharmaceutics.* **14**, 2414 (2022).
53. W. Zeng, Y. Song, R. Wang, R. He, T. Wang, Neutrophil elastase: From mechanisms to therapeutic potential. *J. Pharm. Anal.* **13**, 355–366 (2023).
54. H. Liu, E. M. Lessieur, A. Saadane, S. I. Lindstrom, P. R. Taylor, T. S. Kern, Neutrophil elastase contributes to the pathological vascular permeability characteristic of diabetic retinopathy. *Diabetologia* **62**, 2365–2374 (2019).
55. C. M. Dollery, C. A. Owen, G. K. Sukhova, A. Krettek, S. D. Shapiro, P. Libby, Neutrophil elastase in human atherosclerotic plaques. *Circulation* **107**, 2829–2836 (2003).
56. H. Zhang, Y. Wang, M. Qu, W. Li, D. Wu, J. P. Cata, C. Miao, Neutrophil, neutrophil extracellular traps and endothelial cell dysfunction in sepsis. *Clin. Transl. Med.* **13**, e1170 (2023).
57. H. Shi, A. A. Gandhi, S. A. Smith, Q. Wang, D. Chiang, S. Yalavarthi, R. A. Ali, C. Liu, G. Sule, P.-S. Tsou, Y. Zuo, Y. Kanthi, E. A. Farkash, J. D. Lin, J. H. Morrissey, J. S. Knight, Endothelium-protective, histone-neutralizing properties of the polyanionic agent defibrotide. *JCI insight.* **6**, e149149 (2021).
58. Y. Zuo, S. Yalavarthi, H. Shi, K. Gockman, M. Zuo, J. A. Madison, C. Blair, A. Weber, B. J. Barnes, M. Egeblad, R. J. Woods, Y. Kanthi, J. S. Knight, Neutrophil extracellular traps in COVID-19. *JCI insight.* **5**, e138999 (2020).
59. E. B. Taylor, Casting a wide NET: An update on uncontrolled NETosis in response to COVID-19 infection. *Clin. Sci. (Lond.)* **136**, 1047–1052 (2022).
60. A. R. Thierry, B. Roch, SARS-CoV2 may evade innate immune response, causing uncontrolled neutrophil extracellular traps formation and multi-organ failure. *Clin. Sci. (Lond.)* **134**, 1295–1300 (2020).
61. S. L. Pfister, Role of platelet microparticles in the production of thromboxane by rabbit pulmonary artery. *Hypertension* **43**, 428–433 (2004).
62. J. Rosińska, M. Łukasik, W. Kozubski, The impact of vascular disease treatment on platelet-derived microvesicles. *Cardiovasc. Drugs Ther.* **31**, 627–644 (2017).
63. R. Pakala, Serotonin and thromboxane A2 stimulate platelet-derived microparticle-induced smooth muscle cell proliferation. *Cardiovasc. Radiat. Med.* **5**, 20–26 (2004).
64. C. Ingerman-Wojenski, M. J. Silver, J. B. Smith, E. Macarak, Bovine endothelial cells in culture produce thromboxane as well as prostacyclin. *J. Clin. Invest.* **67**, 1292–1296 (1981).
65. C. Lam, S. Ananth Karumanchi, Pregnancy and the kidney, in *Textbook of Nephro-Endocrinology* (Elsevier, 2009), pp. 483–513.
66. Z. Guo, W. Su, S. Allen, H. Pang, A. Daugherty, E. Smart, M. C. Gong, COX-2 up-regulation and vascular smooth muscle contractile hyperreactivity in spontaneous diabetic db/db mice. *Cardiovasc. Res.* **67**, 723–735 (2005).
67. P. Conti, M. Reale, R. C. Barbacane, M. Bongrazio, M. R. Panara, S. Fiore, R. Dempsey, L. Borish, Leukocyte inhibitory factor activates human neutrophils and macrophages to release leukotriene B4 and thromboxanes. *Cytokine* **2**, 142–148 (1990).
68. M. V. Tahamont, M. H. Gee, J. T. Flynn, Aggregation and thromboxane synthesis and release in isolated sheep neutrophils and lymphocytes in response to complement stimulation. *Prostaglandins Leukot. Med.* **16**, 181–190 (1984).
69. M. L. Eskew, A. Zarkower, W. J. Scheuchenzuber, G. R. Hildenbrandt, R. W. Scholz, C. C. Reddy, Increased thromboxane A2 synthesis by rat lung neutrophils during selenium deficiency. *Prostaglandins* **46**, 319–329 (1993).
70. J. Li, C. Guo, J. Wu, 15-Deoxy-Δ-12,14-prostaglandin J2 (15d-PGJ2), an endogenous ligand of PPAR-γ: Function and mechanism. *PPAR Res.* **2019**, 7242030 (2019).
71. H. Migita, J. Morser, 15-deoxy-$\Delta^{12,14}$-prostaglandin J_2(15d-PGJ2) signals through retinoic acid receptor–related orphan receptor-α but not peroxisome proliferator–activated receptor-γ in human vascular endothelial cells: The Effect of 15d-PGJ2 on tumor necrosis factor-α–induced gene expression. *Arterioscler. Thromb. Vasc. Biol.* **25**, 710–716 (2005).
72. A. T. Coyle, M. B. O'Keeffe, B. T. Kinsella, 15-deoxy $\Delta^{12,14}$-prostaglandin J_2 suppresses transcription by promoter 3 of the human thromboxane A_2 receptor gene through peroxisome proliferator-activated receptor γ in human erythroleukemia cells. *FEBS J.* **272**, 4754–4773 (2005).
73. K. B. Atkins, B. Irey, N. Xiang, F. C. Brosius, A rapid, PPAR-gamma-dependent effect of pioglitazone on the phosphorylation of MYPT. *Am. J. Physiol. Cell Physiol.* **296**, C1151–C1161 (2009).
74. S. B. Gurley, C. L. Mach, J. Stegbauer, J. Yang, K. P. Snow, A. Hu, T. W. Meyer, T. M. Coffman, Influence of genetic background on albuminuria and kidney injury in Ins2(+/C96Y) (Akita) mice. *Am. J. Physiol. Renal Physiol.* **298**, F788–F795 (2010).
75. S. B. Gurley, S. E. Clare, K. P. Snow, A. Hu, T. W. Meyer, T. M. Coffman, Impact of genetic background on nephropathy in diabetic mice. *Am. J. Physiol. - Ren. Physiol.* **290**, 214–222 (2006).
76. L. Wang, Y. Sha, J. Bai, W. Eisner, M. A. Sparks, A. F. Buckley, R. F. Spurney, Podocyte-specific knockout of cyclooxygenase 2 exacerbates diabetic kidney disease. *Am. J. Physiol. Renal Physiol.* **313**, F430–F439 (2017).
77. S. Oyadomari, A. Koizumi, K. Takeda, T. Gotoh, S. Akira, E. Araki, M. Mori, Targeted disruption of the Chop gene delays endoplasmic reticulum stress-mediated diabetes. *J. Clin. Invest.* **109**, 525–532 (2002).
78. C. Le May, K. Chu, M. Hu, C. S. Ortega, E. R. Simpson, K. S. Korach, M.-J. Tsai, F. Mauvais-Jarvis, Estrogens protect pancreatic beta-cells from apoptosis and prevent insulin-deficient diabetes mellitus in mice. *Proc. Natl. Acad. Sci. U.S.A.* **103**, 9232–9237 (2006).
79. J. L. Park, L. Shu, J. A. Shayman, Differential involvement of COX1 and COX2 in the vasculopathy associated with the alpha-galactosidase A-knockout mouse. *Am. J. Physiol. Heart Circ. Physiol.* **296**, H1133–H1140 (2009).
80. R. A. Ali, A. A. Gandhi, L. Dai, J. Weiner, S. K. Estes, S. Yalavarthi, K. Gockman, D. Sun, J. S. Knight, Antineutrophil properties of natural gingerols in models of lupus. *JCI insight.* **6**, e138385 (2021).
81. F. Afshinnia, L. Zeng, J. Byun, S. Wernisch, R. Deo, J. Chen, L. Hamm, E. R. Miller, E. P. Rhee, M. J. Fischer, K. Sharma, H. I. Feldman, G. Michailidis, S. Pennathur, Elevated lipoxygenase and cytochrome P450 products predict progression of chronic kidney disease. *Nephrol. Dial. Transplant.* **35**, 303–312 (2020).

Acknowledgments: This work was supported by The Assistant Secretary of Defense for Health Affairs endorsed by the Department of Defense through the Peer Reviewed Medical Research Program. Opinions, interpretations, conclusions, and recommendations contained herein are those of the author(s) and are not necessarily endorsed by the Department of Defense. In conducting research using animals, the investigators adhered to the laws of the United States and the regulations of the Department of Agriculture. **Funding:** This work was supported by Department of Defense grant W81XWH-20-1-0663 (to J.S.K.) and NIH grant P30 DK89503 (to S.P.). **Author contributions:** Conceptualization: C.L., S.Y., K.B.A., S.P., and J.S.K. Methodology: C.L., S.Y., A.T., L.Z., H.S., and K.B.A. Investigation: C.L., S.Y., A.T., L.Z., C.E.R., N.A., L.H., W.L., and S.K.N. Visualization: C.L., S.Y., A.T., and L.Z. Novel reagents: MAS. Supervision: J.S.K. and S.P. Writing (original draft): C.L. and S.Y. Writing (review and editing): J.S.K., with approval by all authors. **Competing interests:** The authors declare that they have no competing interests. **Data and materials availability:** All data needed to evaluate the conclusions in the paper are present in the paper and/or the Supplementary Materials. The *Pad4*$^{-/-}$ mice on the C57BL/6 background can be provided with the permission of M.A.S. pending scientific review and a completed material transfer agreement. Requests for these mice should be submitted to mshelef@medicine.wisc.edu or jsknight@umich.edu.

Submitted 12 June 2023
Accepted 20 September 2023
Published 25 October 2023
10.1126/sciadv.adj1019